



Materials Science

An Indian Journal

Full Paper

MSAIJ, 14(5), 2016 [169-176]

Microstructural, mechanical and corrosion properties of two simple cast nickel-based alloys derived from a real dental alloy employed in prosthetic dentistry

Lyndho Princilia Billy Nsougui¹, Patrice Berthod^{1,2*}

¹Faculty of Sciences and Technologies, University of Lorraine, B.P. 70239, 54506 Vandoeuvre-lès-Nancy (FRANCE)

²Institut Jean Lamour (UMR CNRS 7198), University of Lorraine, B.P. 70239, 54506 Vandoeuvre-lès-Nancy – (FRANCE)

E-mail: Patrice.Berthod@univ-lorraine.fr

ABSTRACT

Many metallic pieces used in prosthetic dentistry are made of very expensive metals such as gold, platinum, palladium or silver, to guarantee absence of any corrosion phenomena. Much cheaper alloys presenting high ductility and resistance, and simultaneously high corrosion resistance, exists and are of great interest. This is the case of {nickel-chromium}-based alloys containing heavy elements as molybdenum for good mechanical properties and rich enough in chromium to ensure the development of a very protective chromia passivation layer. Other elements such Si or Al may be also present. The purpose of this work is first to study the microstructure, mechanical and corrosion role of silicon in a nickel-based chromium-rich alloy inspired from a commercial dental alloy. Casting, microstructure characterization, mechanical test by indentation and compression, and electrochemical corrosion experiments were carried out for a Si-free and a Si-containing Ni-25.7Cr-11Mo alloys, with also consideration to a possible hardened state by preliminary plastic deformation. The Si effect on the mechanical properties was significant, but not its influence on the corrosion behaviour. This may be due to the very high initial corrosion resistance of these alloys.

© 2016 Trade Science Inc. - INDIA

KEYWORDS

Dental nickel-based alloys;
Silicon;
Microstructure;
Compression;
Hardness;
Corrosion.

INTRODUCTION

Metallic alloys are often employed in dentistry inside prostheses, in association with ceramics. They bring good mechanical resistance and high ductility or toughness what is lacking in cosmetic ceramic the role of which is essentially aesthetical. How-

ever, as metals, these alloys are potentially strengthened by corrosion in the buccal milieu, what explains that the metallic alloys used in dental prostheses are often based on noble elements (Au, Pt, Pd...). Such alloys are necessarily expensive and they are sometimes replaced by much cheaper alloys, for example based on nickel since several decades ago^[1]. De-

Full Paper

spite that biocompatibility^[2] and allergy^[3,4] problems are often evoked about this element, they represent an interesting economic alternative since they may be simultaneously mechanically^[5-9] and corrosion^[10-13] resistant. However their elaboration and shaping may present some possibly problematic specificity (castability^[14], chemical homogeneity^[15], heat-treatments^[16,17]...).

Dental nickel-based alloys are present in the catalogue of various manufacturers besides traditional nobler alloys gold-based or platinum-based for example. This is the case of Ivoclar Vivadent® who proposes, for instance, the Pisces Plus (61.5Ni-22.0Cr-11.2W-2.3Al-2.6Si, in wt.%) and the 4ALL (61.4Ni-25.7Cr-11.0Mo-1.5Si, in wt.%). They both contain Ni as base element and Cr in quantity high enough to allow rapid and robust passivation for a great corrosion resistance. They also contain additional elements W or Mo, and Si or Al, which may influence their response to heat treatment and their resistance to mechanical solicitations and to aqueous corrosion. Varying the chemical composition of the Pisces Plus to study the effect of its microstructure and corrosion properties was previously tested and characterized in a previous work^[18]. The purpose of the present study is to carry out similar tests on the 4ALL this time. This will be done about microstructure and corrosion in a solution simulating saliva, but also on the compression properties. Since hardening will be achieved after elastic deformation, this will allow also observing the effect of plastically deformation on the corrosion behaviour.

EXPERIMENTAL

Elaboration of the alloys

Two alloys were preliminarily elaborated by foundry. Parts of pure elements (Ni, Cr, Mo and Si, mainly from Alfa Aesar, >99.9 wt.%) were separately weighed to obtain about two 40 grams charges each constituted of Cr (25.7 wt.%), Mo (11.0 wt.%) and Ni(rest.), one of the two without any further addition and the second one with additionally 1.5 wt.%Si. Each charge was placed in the water-cooled

crucible of a High Frequency Induction furnace (CELES), which was thereafter isolated from laboratory air by a silica tube in which three cycles { 7×10^{-2} mbar – vacuum; incorporation of 600 mbars of pure Argon} were applied. To finish the internal atmosphere was stabilized to 300 mbars of pure Ar).

Melting of the charge and homogenization were achieved by heating upto about 4kV and almost isothermal stage during three minutes in the liquid state. Rather fast cooling led to solidification and solid state cooling, of a compact ingot.

Machining, metallography preparation and observations

The two ingots were cut in order to obtain different types of samples. Two about {6.5 mm × 5.5 mm × 3 mm}-parallelepipeds were machined in each ingot. In both cases one of the two parts was devoted to metallographic characterization and the second one was kept for specifying the mechanical behaviour compression.

The parts destined for metallography were first embedded in a cold resin mixture (82% of CY230 resin and 18% of HY253 hardener, liquid products from ESCIL®). After total stiffening and extraction outside the plastic mould the obtained mounted samples were ground with SiC papers from 120-grit upto 2400-4000-grit. After ultrasonic cleaning they were polished with textile disk enriched with 1µm hard particles until obtaining a mirror-like state.

The observations were done by electron microscopy. A Scanning Electron Microscope (SEM) from JEOL (JSM 6010LA model), equipped with an Energy Dispersion Spectrometer (EDS), allowed observations in Back Scattered Electrons (BSE) mode and semi-quantitative chemical analysis (full frame and spot), under a 20kV acceleration voltage.

Mechanical properties

The hardness of the two alloys was first specified. This was done by performing Vickers indentation under a 10kg-load, three times per alloy. This allowed obtaining an average value and a standard deviation one.

The parallelepipeds especially machined for that were subjected to compression test allowing a plastic deformation important enough to get a hardened version of the same alloys. Several properties were

deduced from the obtained compression curves: the yield strength (transition from the elastic deformation to the plastic one) and the hardening parameters (k and n) involved in the Ludwig's equation (eq. 1):

$$\sigma = k \times \epsilon^n \quad (1)$$

They can be easily deduced of the straight line resulting from the $\ln(\sigma)$ versus $\ln(\epsilon)$ plotting since the logarithm of k is its ordinate at the origin while n is its slope (eq. 2).

$$\ln(\sigma) = \ln(k) + n \times \ln(\epsilon) \quad (2)$$

Corrosion properties

For each alloy an as-cast parallelepiped part and the plastically deformed parallelepiped parts were immersed in a liquid cold resin mixture but without submersion as for the metallographic samples. After total stiffening they were extracted from the plastic mould. They were placed in a vice, sewed a little and the denuded part of an electrical wire was inserted in the resulting slot by compression. Incorporated again in the mould additional liquid cold resin mixture was poured to totally immerse the upper part of the sample as well as the denuded copper. The metallic part of the obtained electrode was then ground until the 1200-grit paper, washed and dried.

Two types of electrochemical tests were carried out, using the model 263A potentiostat of Princeton Applied Research driven by the M352 software of EGG/Princeton:

Measurement of the Open Circuit potential (E_{ocp}) followed by a linear polarization from $E_{ocp} - 20mV$ up to $E_{ocp} + 20mV$ at the constant rate of $+10mV/min$, to determine the polarization resistance R_p (from the slope of the straight line in the neighbourhood of E_{ocp}). This was done every 10 minutes from $t=0$ and $t=30min$: $t=0$ (immersion of the electrode) $+2$ min (half of experiment since its duration is 4 min), $t=10 + 2$ min (half of experiment) and $t=20 + 2$ min (half of experiment)

Tafel experiment: measurement of the new E_{ocp} than potential increase from $E_{ocp} - 250mV$ up to $E_{ocp} + 1mV/s$ from E_{ocp} at $t=30$ min (duration: from $t=30$ min to $t=30$ min $+500$ seconds). This aimed to specify accurately the values of the corrosion potential (E_{corr}) and of the current density of corrosion (I_{corr}), and also to get the values of the anodic and cathodic Tafel coefficients (β_a and β_c).

These electrochemical experiments were performed in a very simple solution simulating saliva (distilled water added with 9g/L NaCl and pH adjusted to 7.4 just before experiment). Its temperature was maintained at $37^\circ C$ thanks to a special cell allowing the heating by internal fluid circulation from a Julabo F32 device. The Working Electrode (the sample) was 1200-grit ground just before immersion and each electrochemical series of experiments (3 liner polarization and Tafel), the Counter Electrode (or auxiliary electrode) was a platinum one, and the electrode of potential reference was a Saturated Calomel one.

RESULTS AND DISCUSSION

Chemical compositions and microstructures of the obtained alloys; hardness

The chemical compositions of the two alloys are globally well respected (TABLE 1 and TABLE 2). The as-cast microstructure of the NiCrMo alloy is illustrated by SEM/BSE micrographs in Figure 1 (left). It is obviously single-phased but chemical segregations occurred during solidification are

TABLE 1 : Chemical compositions of the NiCrMo alloy (full frame) and of the two distinct areas

NiCrMo alloy	AVERAGE	std deviation
wt.%Ni	62.93	0.50
wt.%Cr	25.82	0.23
wt.%Mo	11.25	0.32
pale areas		
AVERAGE	std deviation	
wt.%Ni	56.26	0.97
wt.%Cr	26.95	0.51
wt.%Mo	16.79	0.49
dark areas		
AVERAGE	std deviation	
wt.%Ni	65.66	0.56
wt.%Cr	24.74	0.39
wt.%Mo	9.59	0.44

Full Paper

TABLE 2 : Chemical compositions of the NiCrMoSi alloy (full frame) and of the two distinct phases

NiCrMoSi alloy	AVERAGE	std deviation
wt.%Ni	61.52	0.27
wt.%Cr	25.36	0.30
wt.%Mo	11.66	0.36
wt.%Si	1.46	0.03
white phase	AVERAGE	std deviation
wt.%Ni	48.61	0.94
wt.%Cr	22.16	0.74
wt.%Mo	25.29	0.29
wt.%Si	3.93	0.37
matrix (pale)	AVERAGE	std deviation
wt.%Ni	59.05	0.80
wt.%Cr	25.41	0.58
wt.%Mo	13.68	1.19
wt.%Si	1.86	0.19
matrix (dark)	AVERAGE	std deviation
wt.%Ni	64.34	0.25
wt.%Cr	25.02	0.15
wt.%Mo	9.74	0.11
wt.%Si	0.90	0.06

clearly visible in the cells' or dendrites' periphery, in which the contents in Cr and especially in Mo are locally high (TABLE 1), with as result a higher average atomic number leading to a clear grey level.

The NiCrMoSi alloy is double-phased in its as-cast state (Figure 1, right). The matrix presents a dark dendrite core with globally the chemical composition of the alloy itself (but a little impoverished in Mo and Si) and a paler periphery in which the Mo and Si contents are, in contrast, a little higher than in the alloy's composition. The white areas, interdendritic and clearly separated from matrix,

constitute a second phase particularly rich in Mo and Si.

Obviously, Mo segregated during solidification, rejected by the growing solid phase into the residual liquid, in both alloys. In the second alloy, the presence of 1.5 wt.%Si promoted the precipitation, in the interdendritic spaces, of a second phase rich in Mo and Si (maybe MoSi_2) at the end of solidification.

The volumes and masses of the samples devoted to the compression tests were exploited to estimate their densities. The values given in TABLE 3 show that there are no real influence, on the density, of the single/double phased structure and of the presence of Si in the chemical composition.

The indentation runs performed on the two alloys led to the values presented in TABLE 4. Seemingly the presence of silicon, and more precisely of the second phase rich in molybdenum and silicon, induced an increase in hardness, with about 30 $\text{Hv}_{10\text{kg}}$ more for the NiCrMoSi alloy in comparison with the silicon-free alloy.

Mechanical properties in compression

The two alloys were subjected to compression test until reaching 6 to 8% of total deformation. The corresponding curves are plotted together in Figure 2. They are rather irregular with curiously two parts of elastic deformation. The values of the yield strengths and of the stresses at which the compression tests were interrupted are given in TABLE 5. The NiCrMoSi alloy seems more resistant against compression than the NiCrMo one (e.g. 40MPa more for the yield strength).

The hardening part of the deformation curves were analysed (Figure 3 and Figure 4) according to (eq. 2) to specify the values of the parameters k and n describing the consolidation phenomenon. The obtained values, given in TABLE 6, suggest that the less elastically resistant alloy (NiCrMo) is in contrast the one which better consolidates (higher values of both k and n). The plastic deformation led to the permanent relative deformations whose values are given in TABLE 7. Along the compression axis the permanent deformation is logically negative, but the absolute values are not the same (-6.3% for NiCrMo and -4.2% for NiCrMoSi). Thus the properties for the two alloys cannot be compared to one

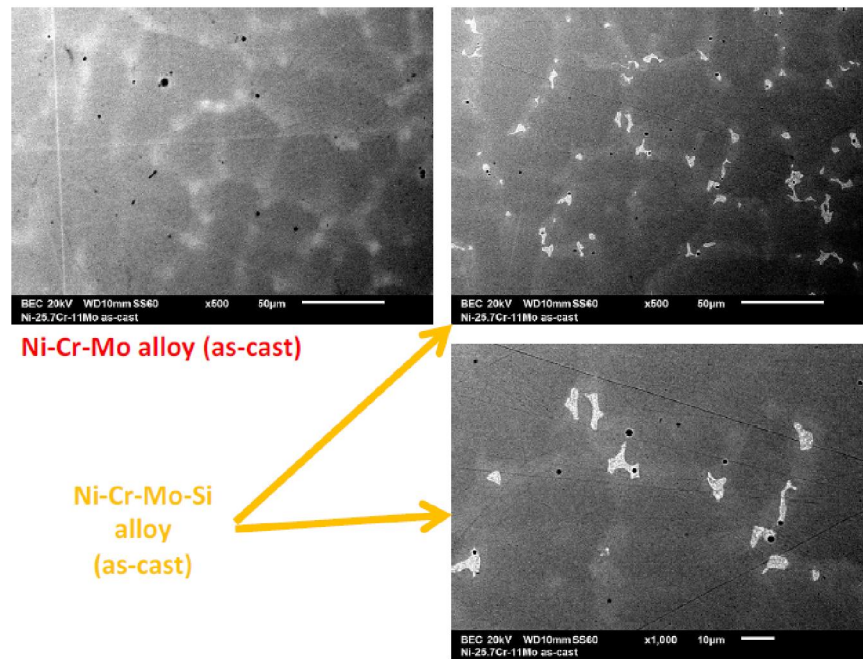


Figure 1 : The microstructures of the two studied alloys as observed with the SEM in BSE mode

TABLE 3 : Estimated values of the densities of the two alloys

NiCrMo alloy	NiCrMoSi alloy in
density (g cm ⁻³)	density (g cm ⁻³)
8.09	8.07

TABLE 4 : Estimated values of the densities of the two alloys

Hardness (Hv10kg)	NiCrMo	NiCrMoSi
AVERAGE	158.4	187.3
Standard deviation	7.6	15.5

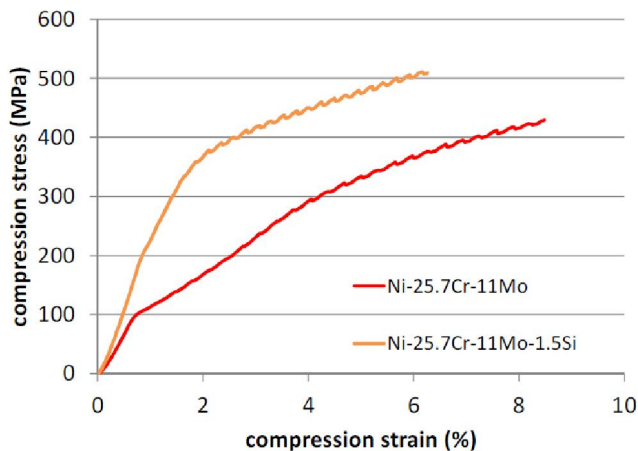


Figure 2 : The compression curves of the two studied alloys

another for the deformed states.

TABLE 5 : The values of the elastic resistance of the alloys and of the maximal stresses at which the the compression were interrupted

NiCrMo alloy	NiCrMoSi alloy
Yield strength (MPa)	
260	306
Maximal stress applied (MPa)	
429	509

TABLE 6 : The values of the parameters of the Ludwig's equation describing the hardening parts of the curves

Hardening constants ($\sigma = k \times \epsilon^n$)	NiCrMo	NiCrMoSi
k (MPa)	1630	1187
n	0.535	0.303

Behaviour in corrosion

The results of linear polarization are displayed in TABLE 8 for the NiCrMo alloy and in TABLE 9 for the NiCrMoSi alloy. One can see first that both alloys are very corrosion-resistant with their very high values of R_p (several hundreds of $k\Omega \times cm^2$). However there is some differences between the two since the resistance of polarization of the NiCrMoSi alloy is lower than the one of the NiCrMo alloy. In contrast the hardening does not seem having a significant effect on the corrosion behaviour of these alloys.

Full Paper

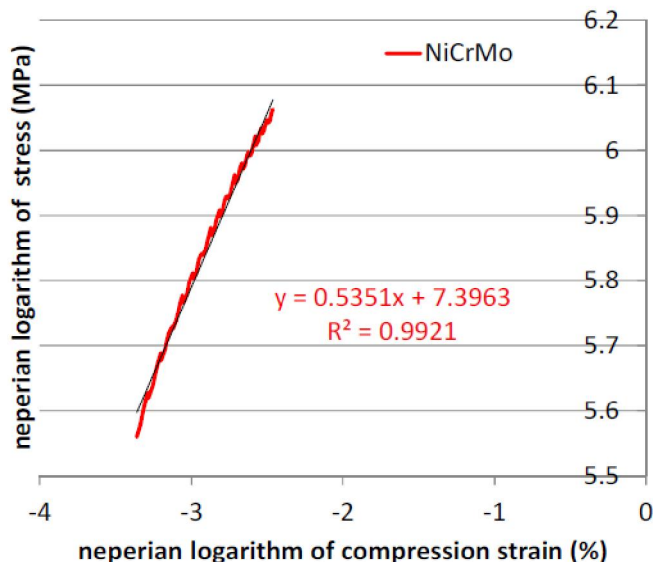


Figure 3 : Determination of the values of the hardening parameters of the NiCrMo alloy

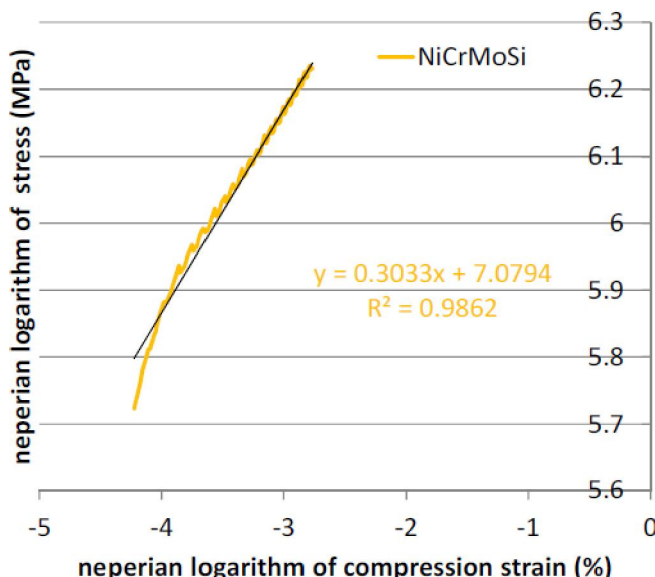


Figure 4 : Determination of the values of the hardening parameters of the NiCrMoSi alloy

The Tafel experiments led to curves which are displayed in Figure 5 (NiCrMo not deformed and in the deformed state), Figure 6 (NiCrMoSi not deformed and in the deformed state) and Figure 7 (NiCrMo and NiCrMoSi in their not deformed state). One can see that the Tafel curves of the initial NiCrMo alloy (i.e. not deformed) and of its plastically deformed version are rather close to one another, even if the current density of corrosion seems smaller for the deformed state (Tafel curve under the other one but slightly shifted in the left direction). The shift of the Tafel curve of the deformed

TABLE 7 : Longitudinal and lateral deformations of the two samples after the deformation tests

Alloy	Relative longitudinal deformation (ϵ_{xx})	Relative Lateral deformations (ϵ_{yy} and ϵ_{zz})
NiCrMo	-6.34%	-1.49% and +0.68%
NiCrMoSi	-4.19%	-0.91% and +3.70%

TABLE 8 : The recorded open circuit potential and measured polarization resistance of the NiCrMo alloy versus time

NiCrMo (ND)	t = 0 min	t = 10 min	t = 20 min
E_{ocp}/HNE (mV)	*	-423.3	-408.0
R_p ($k\Omega \times cm^2$)	*	597.2	768.7

NiCrMo (DF)	t = 0 min	t = 10 min	t = 20 min
E_{ocp}/HNE (mV)	*	-423.0	-408.0
R_p ($k\Omega \times cm^2$)	*	570.4	768.7

TABLE 9 : The recorded open circuit potential and measured polarization resistance of the NiCrMoSi alloy versus time

NiCrMoSi(ND)	t = 0 min	t = 10 min	t = 20 min
E_{ocp}/HNE (mV)	*	-401.9	-395.0
R_p ($k\Omega \times cm^2$)	*	239.7	452.7

NiCrMoSi(DF)	t = 0 min	t = 10 min	t = 20 min
E_{ocp}/HNE (mV)	-588.1	-571.9	-544.6
R_p ($k\Omega \times cm^2$)	101.6	327.9	444.5

NiCrMoSi alloy is in the other direction, with consequently a higher corrosion rate. The most visible difference between these two curves is the significantly lower corrosion potential for the deformed state than for the initial alloy. Concerning the two alloys in their initial (not deformed) versions, the two Tafel curves are almost superposed.

Even if the deformation rates were not exactly the same between the two alloys it was decided to compare their Tafel curves (Figure 8). It appears that the corrosion of the deformed NiCrMoSi is slightly faster than the deformed Si-free version: it was the contrary for the initial not deformed alloys (faster corrosion of the initial NiCrMoSi than for the initial NiCrMo). The numerical values of corrosion potentials and corrosion densities of current, as well as of the anodic and cathodic Tafel coefficients are listed in TABLE 10 for the NiCrMo alloy and in TABLE 11 for the NiCrMoSi one, for their

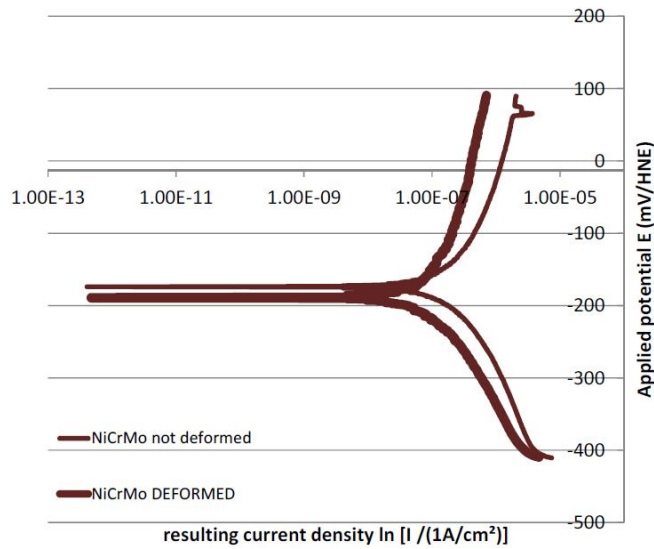


Figure 5 : The Tafel curves obtained for the NiCrMo alloy for its not deformed state and in its deformed state

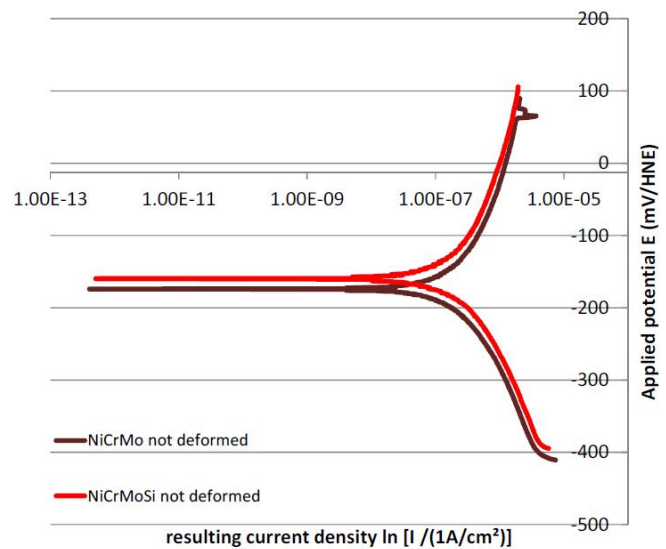


Figure 7 : The Tafel curves obtained for the NiCrMo and NiCrMoSi alloys for in their not deformed states

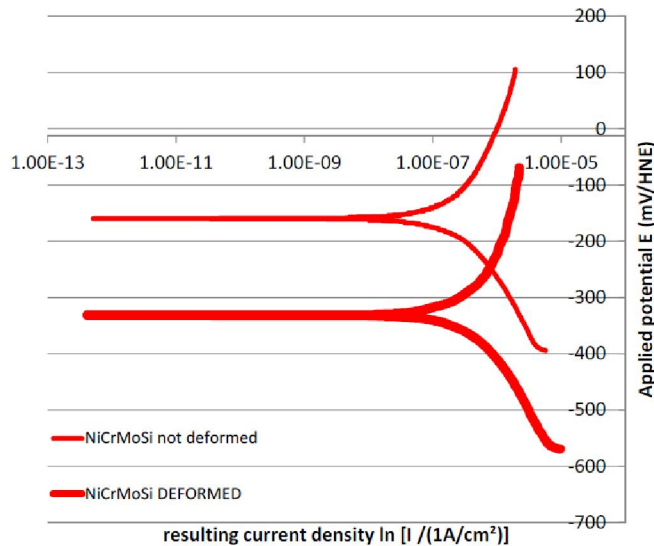


Figure 6 : The Tafel curves obtained for the NiCrMoSi alloy for its not deformed state and in its deformed state

two states.

General commentaries

These two alloys were synthesized in conditions rather different than in the prosthetic reality: solidification much faster by comparison with investment casting, no heat-treatment applied to simulate the thermal cycles imposed to the alloys all along the constitution of a frame work for fixed partial denture for example... However the obtained microstructures were similar to the ones of real dental alloys and the characterization was thus realistic. If the presence of silicon is wished maybe for response of

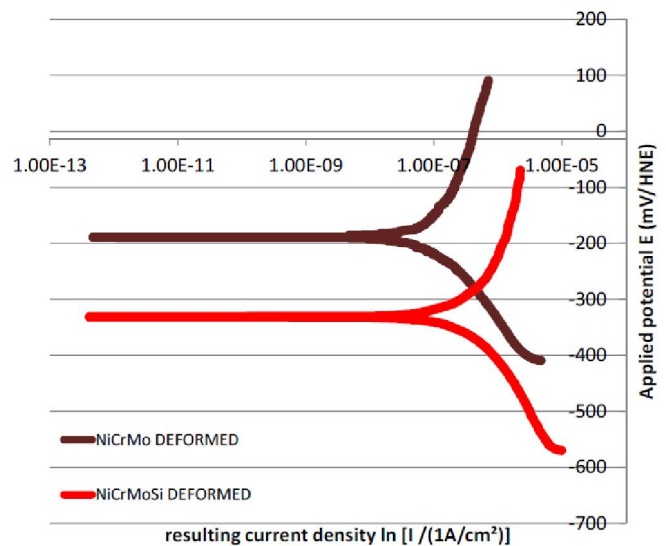


Figure 8 : The tafel curves obtained for the NiCrMo and NiCrMoSi alloys for in their deformed states

the alloy to the “oxidation” treatment ensuring the adhesion between a framework and the ceramic covering, this element, which has consequences on the microstructure, seems also influencing the mechanical properties (hardness, compression) in the good direction. However, concerning the corrosion behavior, the role of silicon is controversial: is there really an interdependence with the plastic deformation? The corrosion currents which were measured are all very low (less than $1 \mu\text{A}/\text{cm}^2$) and these two alloys are clearly both extremely resistant against corrosion. The extremely probable development of a chromia passivation layer in all cases (presence

Full Paper

TABLE 10 : The values of E_{corr} , I_{corr} and of the Tafel anodic and cathodic coefficients for the NiCrMo alloy in its initial state and in its deformed state

NiCrMo Not Deformed			
E_{corr}/ENH (mV)	I_{corr} (nA/cm ²)	β_a (mV/decade)	β_c (mV/decade)
-415.4	368.4	319.5	220.0
NiCrMo Plastically Deformed			
E_{corr}/ENH (mV)	I_{corr} (nA/cm ²)	β_a (mV/decade)	β_c (mV/decade)
-430.3	173.3	497.5	184.2

TABLE 11 : The values of E_{corr} , I_{corr} and of the Tafel anodic and cathodic coefficients for the NiCrMoSi alloy in its initial state and in its deformed state

NiCrMoSi Not Deformed			
E_{corr}/ENH (mV)	I_{corr} (nA/cm ²)	β_a (mV/decade)	β_c (mV/decade)
-399.2	360.8	338.4	210.7
NiCrMoSi Plastically Deformed			
E_{corr}/ENH (mV)	I_{corr} (nA/cm ²)	β_a (mV/decade)	β_c (mV/decade)
-571.7	633.3	392.4	233.5

of Si or not, plastic deformation or not) may be considered as responsible of this excellent behavior, which meets the very good mechanical properties, but which must be possibly to be confirmed by test in other media simulating saliva but more complex and more aggressive.

CONCLUSIONS

Thanks to their chemical composition and microstructures (dendritic Ni-base, heavy atoms in solid solution, eventually Mo-rich and Si-rich particles) the two alloys are mechanically resistant, and with chromium contents high enough, also extremely corrosion resistant with polarization in several tens of kilo-Ohms and corrosion currents lower than the micro-Amperes per cm², whatever the state of the alloy. However it is true that other rates of plastic deformation, remaining realistic with the dental application, remain to be tested. Decreases in Cr also may be to study about the possible consequences in terms of degradation of the corrosion resistance, for example to specify a minimal chromium content under which one must not go. This can be the subject

of extended work.

ACKNOWLEDGMENTS

The authors thank Mathieu Lierre for the preparation of the solution as well as for its assistance.

REFERENCES

- [1] A.J.Lewis; Australian Dental Journal, **20(1)**, 14 (1975).
- [2] J.L.Sandrik, E.J.Kaminski, E.H.Greener; Biomaterials, Medical Devices, And Artificial Organs, **2(1)**, 31 (1974).
- [3] J.P.Nielsen, J.J.Tuccillo; US Patent, US 3340050 19670905, (1967).
- [4] H.F.Hildebrand, C.Veron, P.Martin; Biomaterials, **10(8)**, 545 (1989).
- [5] A.J.Lewis; Australian Dental Journal, **20(2)**, 89 (1975).
- [6] A.J.Lewis; Australian Dental Journal, **22(6)**, 455 (1977).
- [7] K.Wakasa, M.Yamaki, A.Nakatsuka, T.Nishimura; Shika Rikogaku Zasshi, **22(59)**, 217 (1981).
- [8] K.Wakasa, M.Yamaki, A.Nakatuka, T.Nishimura; Shika Rikogaku Zasshi, **22(60)**, 290 (1981).
- [9] T.Yabuki; Jpn.Kokai Tokkyo Koho, Patent JP 63290236 A 19881128, (1988).
- [10] M.Pourbaix; Biomaterials, **5(3)**, 122 (1984).
- [11] G.Tani, F.Zucchi; Minerva Stomatologica, **16(11)**, 710 (1967).
- [12] K.Wakasa, M.Yamaki; Shika Zairyo Kikai, **1(4)**, 339 (1982).
- [13] A.Banu, O.Radovici, M.Marcu; Roumanian Biotechnological Letters, **9(2)**, 1603 (2004).
- [14] K.Wakasa, M.Yamaki; Hiroshima Daigaku Shikagu Zasshi, **13(2)**, 238 (1981).
- [15] A.J.Lewis; Australian Dental Journal, **24(3)**, 171 (1979).
- [16] T.G.Goodall, A.J.Lewis; Australian Dental Journal, **24(4)**, 235 (1979).
- [17] E.E.Wakeel, R.A.Fournelle, V.BDhuru, J.M.Toth; Structural biomaterials for the 21th century, proceedings of the symposium presented at the 2001 TMS annual meeting, New Orleans, LA, United States, Feb.11-12, 2001 (2001).
- [18] L.Janiaut, L.Kedinger, P.Berthod, P.De March; Materials Science: An Indian Journal, **5(4)**, 414 (2009).